

Thirteen pump-probe resonances of the sodium *D1* line

Vincent Wong,* Robert W. Boyd, C. R. Stroud, Jr., Ryan S. Bennink, and Alberto M. Marino
The Institute of Optics, University of Rochester, Rochester, New York 14627, USA

(Received 19 March 2003; published 8 July 2003)

We present the results of a pump-probe laser spectroscopic investigation of the Doppler-broadened sodium *D1* resonance line. We find 13 resonances in the resulting spectra. These observations are well described by the numerical predictions of a four-level atomic model of the hyperfine structure of the sodium *D1* line. We also find that many, but not all, of these features can be understood in terms of processes originating in a two-level or three-level subset of the full four-level model. The processes we observed include forward near-degenerate four-wave mixing and saturation in a two-level system, difference-frequency crossing and nondegenerate four-wave mixing in a three-level *V* system, electromagnetically induced transparency and optical pumping in a three-level lambda system, cross-transition resonance in a four-level double-lambda system, and conventional optical pumping. Most of these processes lead to sub-Doppler or even subnatural linewidths. The dependence of these resonances on the pump intensity and pump detuning from atomic resonance are also studied.

DOI: 10.1103/PhysRevA.68.012502

PACS number(s): 32.30.Jc, 33.40.+f, 42.50.Gy, 32.80.Bx

I. INTRODUCTION

Sodium has played a major role in the development of optical spectroscopy. The resonance line of sodium has been used as a spectroscopic standard because it has a strong transition in the visible portion of the electromagnetic spectrum. The energy-level structure of sodium [1,2] is well known and many nonlinear spectroscopic studies [3–5] have also been performed in sodium.

Historically, sodium has been the medium of choice for verifying new predictions in nonlinear and quantum optics. Optical bistability [6], resonance fluorescence in the presence of a strong driving field [7], coherent population trapping [8], and squeezed light [9] were first observed in sodium. Sodium was also the first atomic system in which various collision-induced processes [10,11] were observed. Other multiphoton resonances were also studied in sodium; they include Raman processes [12], various types of four-wave-mixing processes [13,14], electromagnetically induced transparency (EIT) [15,16], and lasing without inversion [17,18].

These processes are normally studied individually in a pure *N*-level structure, for example, EIT in a three-level lambda (Λ) system without additional adjacent levels. We show here that in the four-level hyperfine structure of the *D1* line of atomic sodium, many different nonlinear processes coexist and are still easily resolvable even though some of these resonances are of subnatural linewidths. The presence of these extremely narrow resonances holds great importance for many applications in optical metrology and the creation of frequency standards of higher precision. Each of the experimentally observed resonances can be explained by considering some subset of the four levels. Fulton *et al.* [19] have seen some of these resonances between hyperfine levels from different *D* lines of rubidium.

In this paper, we describe the dependence of the observed resonances on the pump intensity and detuning from atomic resonance, and a numerical model based on the four-level

hyperfine structure is used to interpret the observations. A subset of the four-level system is used to explain each of the resonances. The Zeeman sublevels are also discussed.

II. EXPERIMENT

We performed a pump-probe experiment with an atomic sodium vapor cell, as illustrated in Fig. 1. The fixed-frequency pump field (ω_{pu}) is produced by a Coherent 699 continuous wave dye laser and a weaker frequency-scanned probe field (ω_{pr}) is produced by another identical dye laser. A Burleigh WA4500 wavemeter monitors the wavelengths of the fields. The pump and probe fields are collimated, copropagating, collinear, and are linearly and orthogonally polarized. Transit time effects¹ are reduced through our use of a pump spot size larger than that of the probe. We achieve this larger spot size by passing the pump field through a telescopic beam expander. The vapor cell is pumped down to 10^{-7} torr and no buffer gas is introduced. The cell is then heated to 152°C creating a number density of 1.6×10^{11} atoms/cm³ with a minimum transmittance of 25% for the probe field in the absence of the pump field. After passing through the cell, the probe is separated from the pump by a polarizing beam splitter and fed to a photodiode.

Curve (a) of Fig. 2 shows the experimental probe transmission spectrum in the absence of the pump field and is included as a reference. Curve (b) is the probe transmission for comparable pump (9.7 mW/cm^2) and probe intensities (1.3 mW/cm^2). Curve (c) is the probe transmission in the presence of a saturating pump field (525 mW/cm^2). Each of the resonances can be explained in terms of a simplified level structure denoted on the top, and the subsystems in which the processes occur are shown on the right-side of Fig. 2.

The sodium *D1* line (589 nm) comprises transitions between either of the two hyperfine ground levels (1772 MHz apart) and either of the two hyperfine excited levels (189

¹Transit time effects can be included as an incoherent dephasing contribution to the Raman transition.

*Electronic address: vin@optics.rochester.edu

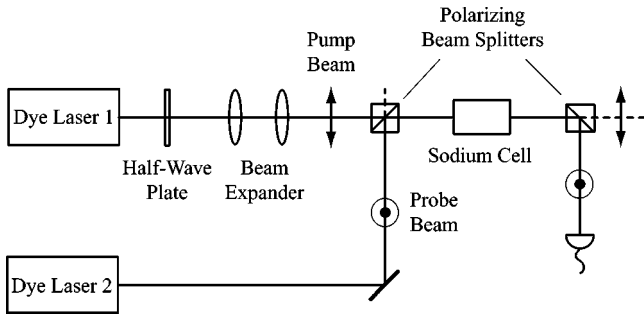


FIG. 1. Physical layout of the pump-probe experiment.

MHz apart) [1]. The pump field is tuned to connect the midpoint of the upper levels to the midpoint of the lower levels. The $D1$ line is Doppler-broadened and is not a pure two-level system, thus the saturation intensity is larger than that for a simple two-level transition.

The two broad transmission dips (labeled S) 1.772 GHz apart result from the single-photon Doppler-broadened transitions between the hyperfine ground levels and the excited levels. These dips have a full-width-at-half-maximum (FWHM) linewidth of 1.5 GHz. The hyperfine excited levels, however, cannot be resolved with a single field because of Doppler broadening. The central transmission peak (T) is a consequence of forward near-degenerate four-wave mixing and saturation in a two-level system. The inner pair of spectral features (V) is a result of saturation and nondegenerate four-wave mixing in a V system. The outer pair of transmission peaks (ΛP), which is most visible in curve (c) of Fig. 2, results from EIT in a Λ system. The broader transmission dip (ΛD) and the pair of satellite dips ($\Lambda\Lambda$) around the EIT peak in curve (b) result from optical pumping. The satellite dips are present only in a double- Λ system.

Because of Doppler broadening of the transition frequency, both the pump and probe fields can excite all of the transitions in the four-level structure. Consequently, each feature except the central peak appears twice, once on either side of the pump frequency. For a given applied field inten-

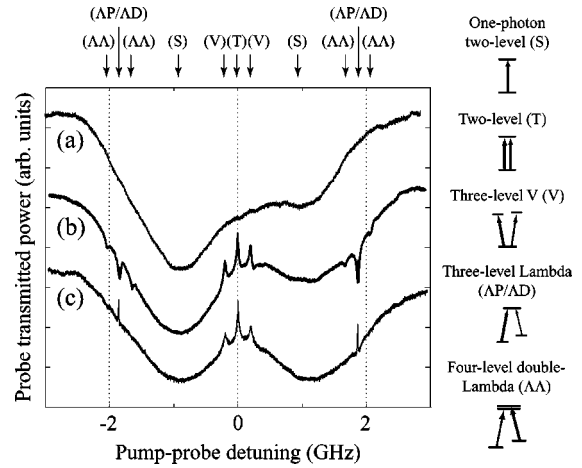


FIG. 2. Probe transmission vs pump-probe detuning for various pump intensities: (a) no pump, (b) weakly saturating pump, 9.7 mW/cm², and (c) saturating pump, 525 mW/cm². The probe intensity is 1.3 mW/cm² for all cases. The resonances are labeled on the top and the subsystems, where the resonances occur, are shown on the right. The spectra in this figure and subsequent ones are displaced vertically for visual clarity.

sity and frequency, the Rabi frequency (due to different dipole strength [2,20]) and the detuning of that field is slightly different for each transition. On the other hand, the particular geometry of the experiment results in an almost complete cancellation of Doppler broadening for the multiphoton transitions. Residual Doppler broadening need only be taken into account when the width of the resonance is very narrow. In addition to this particular geometry, the frequencies of the fields are comparable, therefore phase matching is achieved for the wave-mixing processes.

Two intensity regimes are studied in the experiment. When the pump field is only weakly saturating, all 13 resonances are visible. If the pump intensity is larger than that of the probe field, many of the features wash out and conventional optical pumping is significant. Conventional optical

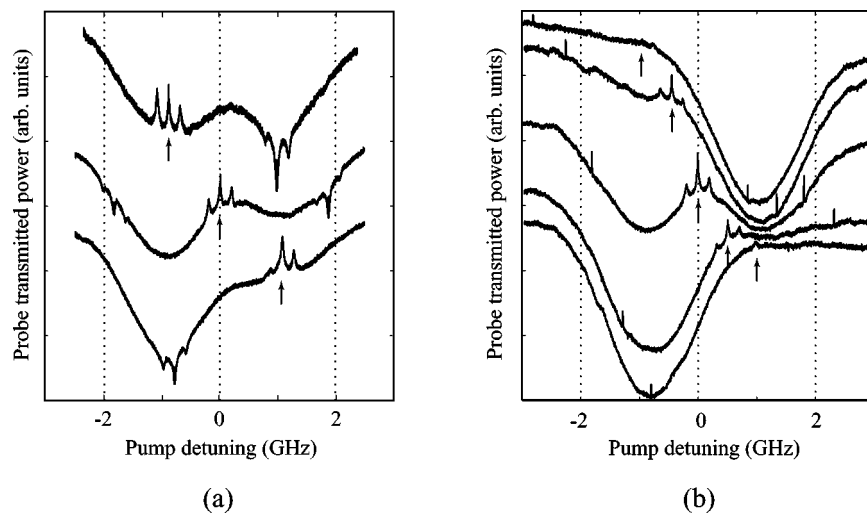


FIG. 3. Probe transmission vs probe detuning for various pump detunings from atomic resonance with (a) a weakly saturating and (b) a saturating pump. The arrow designates the pump frequency in each case.

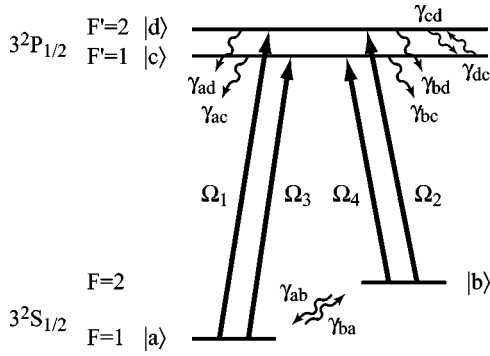


FIG. 4. Energy level diagram of the four-level model.

pumping (to the other hyperfine ground level) effectively reduces population in the subsystem under analysis. Within each regime, power broadening does not modify the features significantly.

As the pump frequency is tuned across the Doppler profile, conventional optical pumping that transfers population from one ground level to the other is evident from the top to the bottom spectra of Figs. 3(a) and 3(b). When the pump field is tuned closer to one of the V (or double- Λ) subsystems, the contributions to the red-detuned and the blue-detuned peaks (dips) are different. The robustness of the EIT signal is clearly seen, as the peak still persists even when in the wings of the Doppler profile. The best condition for observing the two-level and V subsystem resonances occurs when the pump field is tuned between the two hyperfine ground levels (middle spectrum of Fig. 3).

III. THEORETICAL ANALYSIS

A. Four-level system

We model the hyperfine structure of sodium with the four-level system shown in Fig. 4, to interpret our experimental results. The density matrix equations of motion for this system are given by

$$\dot{\tilde{\rho}}_{nn} = -\frac{i}{\hbar} \sum_k (\tilde{V}_{nk} \tilde{\rho}_{kn} - \tilde{\rho}_{nk} \tilde{V}_{kn}) + \sum_{l>n} \gamma_{nl} \tilde{\rho}_{ll} - \sum_{l<n} \gamma_{ln} \tilde{\rho}_{nn}, \quad (1)$$

$$\begin{aligned} \dot{\tilde{\rho}}_{nm} = & -\frac{i}{\hbar} \sum_k (H_{0,nk} \tilde{\rho}_{km} - \tilde{\rho}_{nk} H_{0,km}) \\ & -\frac{i}{\hbar} \sum_k (\tilde{V}_{nk} \tilde{\rho}_{km} - \tilde{\rho}_{nk} \tilde{V}_{km}) \\ & -\frac{1}{2} \left(\sum_{l<n} \gamma_{ln} + \sum_{l<m} \gamma_{lm} \right) \tilde{\rho}_{nm} - \gamma_{nm}^{\text{coll}} \tilde{\rho}_{nm}, \end{aligned} \quad (2)$$

where n , m , k , and l correspond to a , b , c , or d . The interaction Hamiltonian (\tilde{V}) comprises four pairs (pump \tilde{E}_{pu} and probe \tilde{E}_{pr}) of fields corresponding to each of the four transitions, and is represented by

$$\tilde{V}_{da} = \hbar \tilde{\Omega}_1 = -\mu_{da} \tilde{\mathcal{E}}, \quad (3a)$$

$$\tilde{V}_{db} = \hbar \tilde{\Omega}_2 = -\mu_{db} \tilde{\mathcal{E}}, \quad (3b)$$

$$\tilde{V}_{ca} = \hbar \tilde{\Omega}_3 = -\mu_{ca} \tilde{\mathcal{E}}, \quad (3c)$$

$$\tilde{V}_{cb} = \hbar \tilde{\Omega}_4 = -\mu_{cb} \tilde{\mathcal{E}}, \quad (3d)$$

where

$$\tilde{\mathcal{E}} = (E_{\text{pu}} e^{-i\omega_{\text{pu}} t} + E_{\text{pr}} e^{-i\omega_{\text{pr}} t}). \quad (4)$$

The decay rates between hyperfine excited levels (γ_{cd} and γ_{dc}) and between hyperfine ground levels (γ_{ab} and γ_{ba}) are nonradiative and much smaller than the spontaneous emission rates of the optical transitions (γ_{ad} , γ_{bd} , γ_{ac} , and γ_{bc}). Consistent with our experimental condition of low sodium density and no buffer gas, we ignore collisional broadening ($\gamma_{nm}^{\text{coll}}$) in our theoretical model (see the Appendix for the complete equations of motion).

A rotating-frame transformation followed by a Fourier analysis of each off-diagonal density matrix element of interest is performed as in Ref. [21] for the numerical simulation. The atomic response of the probe field is calculated to first order, while the response of the pump field is calculated exactly. The density matrix element obtained for a single atom is averaged over a Maxwellian profile to take Doppler broadening into account.

Each hyperfine level consists of multiple Zeeman magnetic sublevels. Since stray magnetic fields are negligible under our experimental conditions, these sublevels are nearly degenerate. A brief discussion on the effects of stray magnetic fields is presented in Sec. IV. By using orthogonal linear polarizations for the fields, the effect of optical pumping into other Zeeman sublevels is minimized [2]. Therefore, the Zeeman sublevels are ignored in the model. Pump depletion effects and intensity variations across the beams are also neglected in the present theoretical analysis. The other parameters used in the numerical simulation correspond to those of the experimental setup.

We next describe each resonance using a simplified elementary-system model. We also compare the numerical spectra with the experimental ones.

B. Forward near-degenerate four-wave mixing and saturation in a two-level subsystem

The central degenerate transmission peak labeled T in Fig. 5 consists of two features: a 2-MHz FWHM subnatural-linewidth peak superposed on a broader 45-MHz-wide feature. The narrower peak can be understood as a forward near-degenerate four-wave-mixing (FDFWM) process in an open two-level subsystem, as depicted in Fig. 6. An idler photon is generated with the absorption of two pump photons and the emission of one probe photon.

This peak appears only if there is an additional dephasing or a decay (for example, to an external reservoir as in an open system) [22]. In the presence of additional decay paths, narrowing of the resonance below the natural linewidth oc-

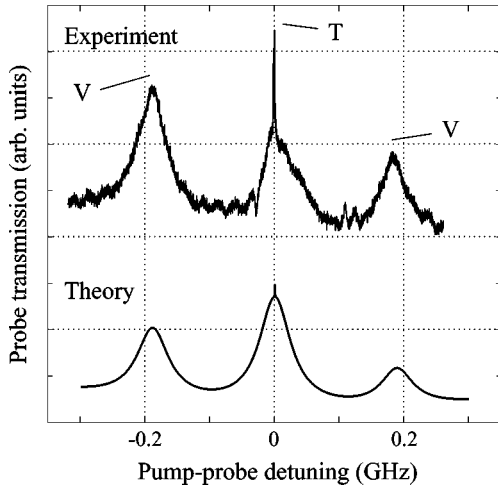


FIG. 5. Resonances associated with the two-level and three-level V subsystems for the case of comparable pump and probe intensities. The theoretical spectrum does not include the idler field of either the two-level FDFWM process or the three-level NDFWM process.

curs only if the additional decay rate for the excited level is larger than the additional decay rate of the ground level. In our experiment, decays to the other hyperfine ground level $|b\rangle$ provide the additional decay channels. The additional excited level decay is governed by spontaneous emission, which is larger than that of the ground level. This satisfies the requirement for resonance narrowing ($\gamma_c > \gamma_a$).

The width of this feature depends on the decay rate of the ground level out of the two-level subsystem (γ_a). Processes contributing to this width are thermal redistribution, the relative dephasing rate between the two lasers, residual Doppler broadening, and diffusion of atoms into and out of the interaction region. In the present experiment, transit time effects are the dominant contribution of this linewidth.

The idler field is of the same polarization as the probe field and both fields are polarized orthogonally to the pump field. As such, the detector measures both the probe and idler fields.

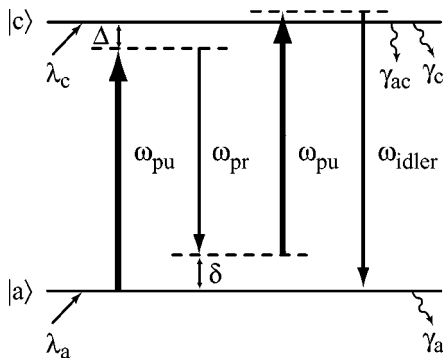


FIG. 6. Four-wave mixing in an open two-level subsystem. Each of the two levels has a small decay rate (γ_i) out of the two-level subsystem and a small repopulation rate (λ_i). Δ is the pump detuning and δ is the pump-probe detuning.

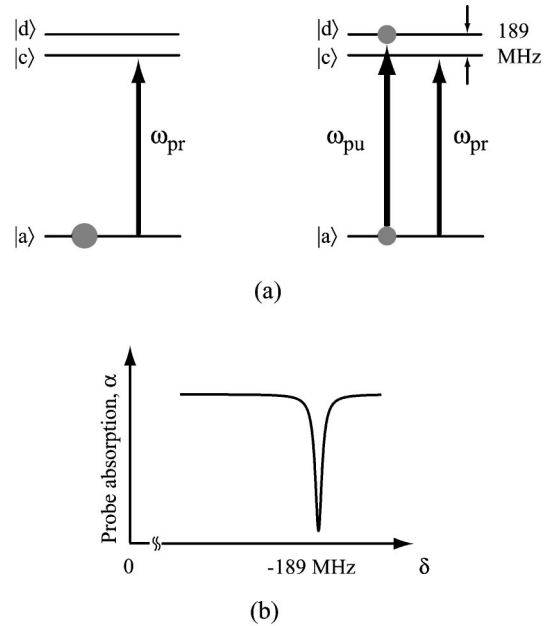


FIG. 7. Difference-frequency crossing resonance in a V subsystem. (a) Energy level diagrams showing the V subsystem. The left (right)-side diagram is in the absence (presence) of the pump field. The population in the level is denoted by the size of the circle. (b) Resulting absorption dip for a red-detuned probe. δ is the pump-probe detuning and α is the probe absorption in the presence of the pump field for a particular velocity subgroup of atoms [Eq. (6)].

The broader peak is a consequence of saturation in a Doppler-broadened medium. The width is power broadened to a few times the radiative linewidth ($1/T_1$).

C. Difference-frequency crossing and nondegenerate four-wave mixing in a V subsystem

The pair of 45-MHz-wide transmission peaks labeled V in Fig. 5, 189 MHz away from the central peak, occurs as a result of saturation and four-wave mixing in a V subsystem. This effect occurs when the frequency difference of the pump and probe fields matches the frequency separation of the excited levels.

With the help of Fig. 7 we may understand the saturation effect, which is a difference-frequency crossing (DFC) resonance, as follows. The probe attenuation is a product of two factors: the absorption cross section and the population of ground level $|a\rangle$. The absorption cross section depends on the probe field's detuning in the usual way, peaking when the probe field is resonant with the $|a\rangle \rightarrow |c\rangle$ transition. The pump field saturates the system when it is resonant with the $|a\rangle \rightarrow |d\rangle$ transition. This causes the ground-level population to be partially depleted [as illustrated by the size of the circle in each level in Fig. 7(a)]. In a Doppler-broadened medium, each factor is resonant for some velocity subgroup of atoms. If $|\omega_{pr} - \omega_{pu}| = \omega_{dc}$, then the resonance in the ground-level depletion occurs for the velocity subgroup that has the largest absorption cross section. This double resonance makes the dominant contribution to the probe absorption, as seen in Fig. 7(b), and the transmission is increased. But if $|\omega_{pr} - \omega_{pu}| \neq \omega_{dc}$, the resonance of the ground-level depletion

occurs for a velocity subgroup that has a low absorption cross section, and the impact of ground-level depletion on the absorption is negligible.

This feature can be understood mathematically as

$$\alpha(\omega_{\text{pr}} - \omega_{\text{pu}} - \omega_{\text{dc}}) = \int N \sigma(\omega_{\text{pr}} - \omega_{\text{ca}} - kv) \times \rho_{aa}(\omega_{\text{pu}} - \omega_{\text{da}} - kv) g(kv) d(kv), \quad (5)$$

where α is the probe absorption in the presence of the pump field, N is the number of atoms, σ is the absorption cross section, ρ_{aa} is the population of ground level $|a\rangle$, and g is the Maxwellian Doppler profile. For simplicity the fields are assumed to be tuned close to resonance, so that only small values of kv are relevant, and $g(kv)$ can be ignored. It has been shown in Ref. [23] that as long as $|\delta - \omega_{\text{dc}}| \ll kv$, where $\delta = \omega_{\text{pr}} - \omega_{\text{pu}}$ is the pump-probe detuning, the fields can be detuned appreciably from their individual transitions (Doppler half width) without affecting the size of the nonlinear polarization. Equation (5) can then be written as a convolution function

$$\alpha(\Delta') = N \int \sigma(\Delta' + \Delta) \rho_{aa}(\Delta) d\Delta, \quad (6)$$

where $\Delta' = \delta - \omega_{\text{dc}}$ and $\Delta = \omega_{\text{pu}} - \omega_{\text{da}} - kv$.

When the probe field is blue detuned from the pump field (pump on the $|a\rangle \rightarrow |c\rangle$ transition, and probe on the $|a\rangle \rightarrow |d\rangle$ transition), the other absorption dip (at +189 MHz) is obtained. The linewidth of the resonance is the sum of those of the two functions (σ and ρ_{aa}) in the integral. In the limiting case of only radiative broadening, both σ and ρ_{aa} are Lorentzians with a linewidth of 10 MHz. The linewidth of the DFC resonance will, therefore, be 20 MHz. The Lorentzians are replaced with their power-broadened versions for larger field intensities.

This DFC resonance is the nondegenerate (in laser frequency), copropagating analog of the crossover resonance studied in Ref. [24]. Our analysis is similar to that of Schlossberg and Javan [23] [see Eq. (21) for traveling waves], and Feld and Javan in their section on a V system [see Eq. (54) of Ref. [25]].

However, the process of DFC does not account completely for these transmission peaks. The experimental curve of Fig. 5 shows one of the V subsystem peaks being stronger than the (broad) saturation peak of the two-level subsystem. For each hyperfine ground level, the two-level saturation process can couple to two velocity subgroups, one for each transition to an excited hyperfine level. The DFC process, however, is resonant with only one velocity subgroup. Therefore, the DFC peak will never be larger than the two-level saturation peak regardless of where the pump field is tuned.

Nondegenerate four-wave mixing (NDFWM) in the V subsystem makes the other contribution. The doubly resonant ($\delta = \omega_{\text{dc}}$) idler field peaks when the pump-probe detuning matches the frequency separation of the excited levels, as shown in Fig. 8. As with the FDFWM case in the two-level

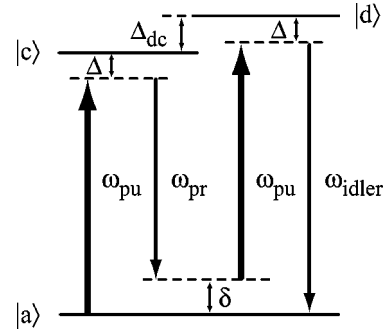


FIG. 8. Four-wave mixing in the V subsystem. The idler peaks when the pump-probe detuning δ matches the excited levels' frequency separation Δ_{dc} .

subsystem, the detector measures both the probe and the idler fields. But unlike the FDFWM peak, there are no line narrowing effects and the width of the resonance is of the order of the homogeneous linewidth that power broadens to a lesser extent than the DFC feature. When the pump intensity is increased the resonance due to DFC washes out partially, leaving mainly the NDFWM contribution.

D. Electromagnetically induced transparency and optical pumping in a Λ subsystem

The most striking manifestation of EIT [26] is the dark state in a Λ system, which is illustrated in Fig. 9(a). When two fields are tuned to a Raman resonance a coherent superposition of the ground states, called a dark state [27], is created. This dark state is decoupled from the excited state resulting in transparency for both fields. The dark state and the orthogonal bright state are given, respectively, by [28]

$$|D\rangle = \frac{\Omega_{\text{pr}}}{\Omega'} |a\rangle - \frac{\Omega_{\text{pu}}}{\Omega'} |b\rangle, \quad (7)$$

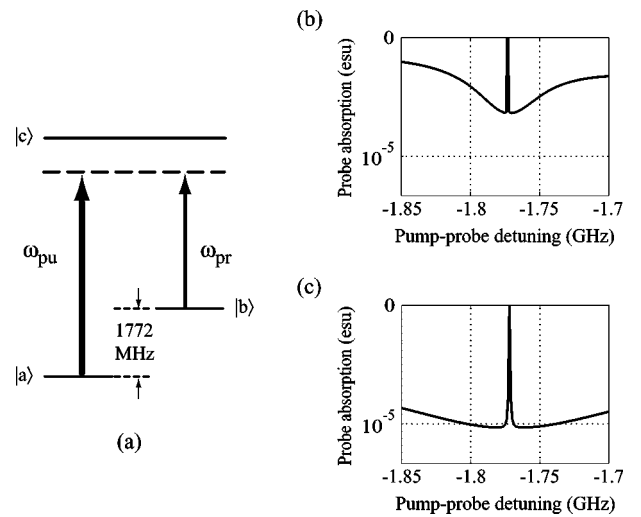


FIG. 9. EIT in a Λ subsystem. (a) Energy level diagram. Also shown are the theoretical probe absorption spectra with (b) a weakly saturating and (c) a saturating pump field. The broad enhanced absorption feature occurs due to optical pumping. Note that the absorption ($\text{Im } \chi^{(1)}$) is increasing downwards.

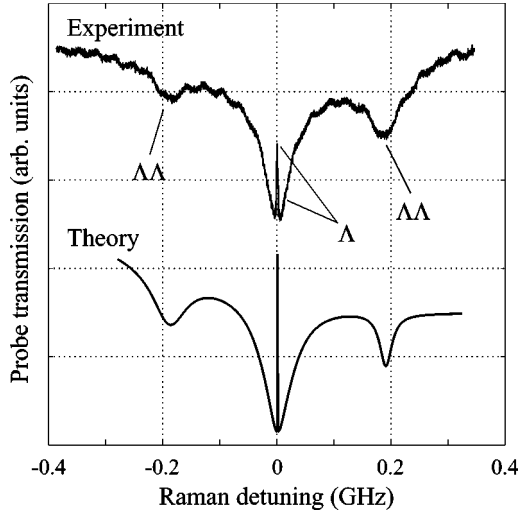


FIG. 10. Resonances associated with the Λ and double Λ sub-systems for the case of comparable pump and probe intensities.

$$|B\rangle = \frac{\Omega_{\text{pr}}}{\Omega'}|a\rangle + \frac{\Omega_{\text{pu}}}{\Omega'}|b\rangle, \quad (8)$$

where $\Omega' = \sqrt{\Omega_{\text{pu}}^2 + \Omega_{\text{pr}}^2}$ and Ω_{pu} (Ω_{pr}) is the Rabi frequency of the pump (probe) field. This transparency results from a destructive interference between the two pathways to the excited state. The linewidth of the EIT feature is dependent on the decoherence rate between the two ground states, and not on the decay rate of the radiative transitions, which can be much larger. This decoherence rate is affected by the same factors that determine the decay rate of the lower level out of the two-level subsystem described earlier. The decay rate of the dark state in a Λ system is, therefore, smaller than that of the corresponding states in a cascade or V system.

Even though there are two close-lying excited levels in the hyperfine structure, it has been shown that the extra off-resonant level only slightly perturbs the EIT system and modifies only the phase of each field component [29]. By tuning to the center of gravity of the set of hyperfine levels that constitute one of the levels of the Λ system, EIT can be achieved just as in a pure three-level Λ system [30]. EIT has also been observed using circularly polarized fields to couple particular Zeeman sublevels [31].

The EIT feature is illustrated in Figs. 9(b) and 9(c). If the intensity of the pump field is comparable to that of the probe field, a 45-MHz-wide broad absorption feature centered on the 2-MHz-wide EIT transmission peak is present (see also Fig. 10). When the pump intensity is increased, the broad transmission dip washes out. This dip has a similar origin as the resonance described in the following section.

E. Cross-transition resonance in a double- Λ system

In Fig. 10, we see a pair of 45-MHz-wide satellite transmission dips symmetrically displaced by 189 MHz from the central EIT feature. These two transmission dips as well as the broad dip centered on the EIT feature are inverted DFC resonances caused by optical pumping in addition to satura-

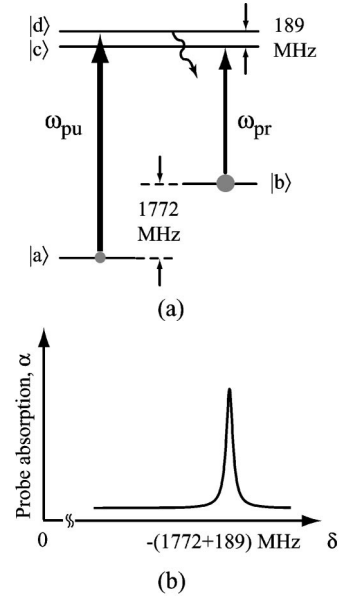


FIG. 11. Cross-transition resonance in a double- Λ system. (a) Energy level diagram showing population (denoted by the size of the circle) being pumped from ground level $|a\rangle$ to ground level $|b\rangle$ through spontaneous emission. (b) Enhanced probe absorption in the presence of the pump field (as described in the text).

tion. For distinction, we shall refer to the satellite pair as cross-transition resonances, that occur only in a double- Λ system. Unlike the usual double- Λ system analyses that include at least three fields, here there are only two, and the transitions they couple do not share a common initial or final level, as illustrated in Fig. 11(a).

As in Sec. III C, the pump field is taken to be tuned to the $|a\rangle \rightarrow |d\rangle$ transition but now the probe field is tuned to the $|b\rangle \rightarrow |c\rangle$ transition. EIT does not occur because the fields are resonant (for a particular velocity subgroup of atoms) with different excited levels. For this velocity subgroup, the pump field drives population to the excited state, which can decay spontaneously to the other ground level ($|b\rangle$). Since the probe field is weaker, the population accumulates in level $|b\rangle$, thereby increasing the population difference ($\rho_{bb} - \rho_{cc}$) of the probe transition or equivalently the probe absorption. The absorption peak shown in Fig. 11(b) is obtained at the pump-probe detuning of the frequency difference between the two transitions, $-(1772+189)$ MHz. The other three cross-transition resonances are obtained in the same fashion.

Similar to the DFC resonance, the width of the cross-transition resonance is also the sum of the widths of the two relevant functions: the absorption cross section σ and the population of level $|b\rangle$, ρ_{bb} . Optical pumping lowers the saturation intensity [5] of the cross-transition resonances as well as the broad dip centered on the EIT feature. Therefore, these resonances wash out much more quickly than the DFC resonances with increasing pump intensity, as can be seen in the bottom curve of Fig. 2.

IV. DISCUSSION

Even weak magnetic fields can sometimes lead to subtle but important effects [32,33]. In the current experiment the

influence of weak stray magnetic fields has been ignored up to this point, but it can manifest itself in two ways: (1) optical pumping or other coherence effects between any of these Zeeman sublevels can modify the strength of the features; (2) the subnatural-linewidth features are broadened.

A narrow resonance can be obtained from coherence between the Zeeman sublevels in a degenerate two-level system as analyzed by Lezama, see Eq. (20) of Ref. [34]. EIT in a Λ system formed between the Zeeman sublevels in the same hyperfine level can enhance the FDFWM peak, which is not included in the theoretical spectrum of Fig. 5. On the other hand, when the pump field is connecting the $F=2 \rightarrow F=1$ transition and the probe connecting the $F=2 \rightarrow F=2$ transition, residual absorption can occur because of optical pumping effects into the extreme Zeeman sublevels ($m_F = \pm 2$) that do not form a V system. Stray magnetic fields will broaden the subnatural-linewidth features of FDFWM and EIT (experimental curve of Figs. 5 and 10) because the Zeeman sublevels are not exactly degenerate anymore. Background absorption countering EIT occurs when the fields are coupled in an off-Raman-resonance manner.

Most of the features observed in this study involve strong modification of the atomic properties. Nonetheless, to the order of magnitude, we can describe the strength of the EIT feature in terms of an n_2 or $\chi^{(3)}$ response. We describe the change in absorption as $\Delta\alpha = 2\Delta n''\omega/c$, where $\Delta n''$ is the change in the imaginary part of the refractive index. Using the definition $\Delta n = n_2 I$, and the observation [see Fig. 2(c)] that the absorption changes by approximately 20% from the typical value of 0.14 cm^{-1} in the presence of a pump field of intensity 10 mW/cm^2 , we find that $\text{Im } n_2 = 1.1 \times 10^{-3} \text{ cm}^2/\text{W}$ or that $\text{Im } \chi^{(3)} = 2.8 \times 10^{-2} \text{ esu}$. The nonlinear response per atom $\gamma^{(3)}$ is $\chi^{(3)}/N$ where $N = 10^{11} \text{ atoms/cm}^3$. The imaginary part of the response is $\text{Im } \gamma^{(3)} = 2.8 \times 10^{-13} \text{ esu}$. By comparison, the measured nonlinear response in a Bose-Einstein condensate [35], with the inclusion of an additional Stark shift, is $\text{Im } n_2 = 0.18 \text{ cm}^2/\text{W}$, $\text{Im } \chi^{(3)} = 4.5 \text{ esu}$, and $\text{Im } \gamma^{(3)} = 5.6 \times 10^{-14} \text{ esu}$.

V. CONCLUSION

Multiple resonances are observed on the Doppler-broadened $D1$ line of atomic sodium in a pump-probe spectroscopic experiment. Each of these resonances can be explained in terms of simple physical processes involving a four-level atomic system or a subset of this system. These resonances arise from various saturation effects (with sub-Doppler linewidth) and various atomic coherence effects (with subnatural linewidth). It should be pointed out that many of the narrow spectral features described in the present and other papers are basically the consequence of some form of optical pumping [36,37]. The dependence of these resonances on the pump intensity and detuning from atomic resonance is also studied. The Zeeman sublevels are found to enhance one transmission peak while contributing to the background absorption and diminishing of other peaks.

ACKNOWLEDGMENTS

This work was supported by the Office of Naval Research under award N00014-02-1-0797 and the U.S. Department of Energy under award DE-FG02-01ER15156.

APPENDIX

The density matrix equations of motion for the four-level double- Λ system, as shown in Fig. 4, are explicitly written as

$$\begin{aligned} \dot{\tilde{\rho}}_{dd} = & -\frac{i}{\hbar}(\tilde{V}_{da}\tilde{\rho}_{ad} - \tilde{\rho}_{da}\tilde{V}_{ad} + \tilde{V}_{db}\tilde{\rho}_{bd} - \tilde{\rho}_{db}\tilde{V}_{bd}) \\ & -(\gamma_{ad} + \gamma_{bd} + \gamma_{cd})\tilde{\rho}_{dd} + \gamma_{dc}\tilde{\rho}_{cc}, \end{aligned} \quad (\text{A1})$$

$$\begin{aligned} \dot{\tilde{\rho}}_{cc} = & -\frac{i}{\hbar}(\tilde{V}_{ca}\tilde{\rho}_{ac} - \tilde{\rho}_{ca}\tilde{V}_{ac} + \tilde{V}_{cb}\tilde{\rho}_{bc} - \tilde{\rho}_{cb}\tilde{V}_{bc}) \\ & + \gamma_{cd}\tilde{\rho}_{dd} - (\gamma_{ac} + \gamma_{bc} + \gamma_{dc})\tilde{\rho}_{cc}, \end{aligned} \quad (\text{A2})$$

$$\begin{aligned} \dot{\tilde{\rho}}_{bb} = & -\frac{i}{\hbar}(\tilde{V}_{bd}\tilde{\rho}_{db} - \tilde{\rho}_{bd}\tilde{V}_{db} + \tilde{V}_{bc}\tilde{\rho}_{cb} - \tilde{\rho}_{bc}\tilde{V}_{cb}) \\ & + \gamma_{bd}\tilde{\rho}_{dd} + \gamma_{bc}\tilde{\rho}_{cc} - \gamma_{ab}\tilde{\rho}_{bb} + \gamma_{ba}\tilde{\rho}_{aa}, \end{aligned} \quad (\text{A3})$$

$$\begin{aligned} \dot{\tilde{\rho}}_{aa} = & -\frac{i}{\hbar}(\tilde{V}_{ad}\tilde{\rho}_{da} - \tilde{\rho}_{ad}\tilde{V}_{da} + \tilde{V}_{ac}\tilde{\rho}_{ca} - \tilde{\rho}_{ac}\tilde{V}_{ca}) + \gamma_{ad}\tilde{\rho}_{dd} \\ & + \gamma_{ac}\tilde{\rho}_{cc} + \gamma_{ab}\tilde{\rho}_{bb} - \gamma_{ba}\tilde{\rho}_{aa}, \end{aligned} \quad (\text{A4})$$

$$\begin{aligned} \dot{\tilde{\rho}}_{da} = & -\frac{i}{\hbar}(H_{0,dd}\tilde{\rho}_{da} - \tilde{\rho}_{da}H_{0,aa}) - \frac{i}{\hbar}(-\tilde{\rho}_{dd}\tilde{V}_{da} - \tilde{\rho}_{dc}\tilde{V}_{ca} \\ & + \tilde{V}_{db}\tilde{\rho}_{ba} + \tilde{V}_{da}\tilde{\rho}_{aa}) - \frac{1}{2}(\gamma_{ad} + \gamma_{bd} + \gamma_{cd} + \gamma_{ba})\tilde{\rho}_{da}, \end{aligned} \quad (\text{A5})$$

$$\begin{aligned} \dot{\tilde{\rho}}_{db} = & -\frac{i}{\hbar}(H_{0,dd}\tilde{\rho}_{db} - \tilde{\rho}_{db}H_{0,bb}) - \frac{i}{\hbar}(-\tilde{\rho}_{dd}\tilde{V}_{db} - \tilde{\rho}_{dc}\tilde{V}_{cb} \\ & + \tilde{V}_{da}\tilde{\rho}_{ab} + \tilde{V}_{db}\tilde{\rho}_{bb}) - \frac{1}{2}(\gamma_{ad} + \gamma_{bd} + \gamma_{cd} + \gamma_{ab})\tilde{\rho}_{db}, \end{aligned} \quad (\text{A6})$$

$$\begin{aligned} \dot{\tilde{\rho}}_{ca} = & -\frac{i}{\hbar}(H_{0,cc}\tilde{\rho}_{ca} - \tilde{\rho}_{ca}H_{0,aa}) - \frac{i}{\hbar}(-\tilde{\rho}_{cd}\tilde{V}_{da} - \tilde{\rho}_{cc}\tilde{V}_{ca} \\ & + \tilde{V}_{ca}\tilde{\rho}_{aa} + \tilde{V}_{cb}\tilde{\rho}_{ba}) - \frac{1}{2}(\gamma_{ac} + \gamma_{bc} + \gamma_{dc} + \gamma_{ba})\tilde{\rho}_{ca}, \end{aligned} \quad (\text{A7})$$

$$\begin{aligned} \dot{\tilde{\rho}}_{cb} = & -\frac{i}{\hbar}(H_{0,cc}\tilde{\rho}_{cb} - \tilde{\rho}_{cb}H_{0,bb}) - \frac{i}{\hbar}(-\tilde{\rho}_{cd}\tilde{V}_{db} - \tilde{\rho}_{cc}\tilde{V}_{cb} \\ & + \tilde{V}_{ca}\tilde{\rho}_{ab} + \tilde{V}_{cb}\tilde{\rho}_{bb}) - \frac{1}{2}(\gamma_{ac} + \gamma_{bc} + \gamma_{dc} + \gamma_{ab})\tilde{\rho}_{cb}, \end{aligned} \quad (\text{A8})$$

$$\begin{aligned} \dot{\tilde{\rho}}_{dc} = & -\frac{i}{\hbar}(H_{0,dd}\tilde{\rho}_{dc}-\tilde{\rho}_{dc}H_{0,cc}) \\ & -\frac{i}{\hbar}(\tilde{V}_{da}\tilde{\rho}_{ac}-\tilde{\rho}_{ca}\tilde{V}_{ac}+\tilde{V}_{db}\tilde{\rho}_{bc}-\tilde{\rho}_{db}\tilde{V}_{bc}) \\ & -\frac{1}{2}(\gamma_{ad}+\gamma_{bd}+\gamma_{cd}+\gamma_{ac}+\gamma_{bc}+\gamma_{dc})\tilde{\rho}_{dc}, \quad (\text{A9}) \end{aligned}$$

$$\begin{aligned} \dot{\tilde{\rho}}_{ab} = & -\frac{i}{\hbar}(H_{0,aa}\tilde{\rho}_{ab}-\tilde{\rho}_{ab}H_{0,bb})-\frac{i}{\hbar}(\tilde{V}_{ad}\tilde{\rho}_{db}-\tilde{\rho}_{ad}\tilde{V}_{db} \\ & +\tilde{V}_{ac}\tilde{\rho}_{cb}-\tilde{\rho}_{ac}\tilde{V}_{cb})-\frac{1}{2}(\gamma_{ba}+\gamma_{ab})\tilde{\rho}_{ab}, \quad (\text{A10}) \end{aligned}$$

and $\dot{\tilde{\rho}}_{ij}=\tilde{\rho}_{ji}^*$. $H_{0,ij}=\hbar\omega_{ij}$, \tilde{V}_{ij} is as defined in Eqs. (3), and γ_{ij} is the population decay rate from level $|j\rangle$ to $|i\rangle$.

-
- [1] F. Schuda, Ph.D. thesis, University of Rochester, Rochester, NY, 1974.
- [2] P. Hemmer, Ph.D. thesis, Massachusetts Institute of Technology Cambridge, MA, 1984.
- [3] A. Corney, *Atomic and Laser Spectroscopy* (Oxford University Press, Oxford, 1977).
- [4] S. Haroche and F. Hartmann, Phys. Rev. A **6**, 1280 (1972).
- [5] M. Levenson, *Introduction to Nonlinear Laser Spectroscopy* (Academic Press, New York, 1982).
- [6] H. Gibbs, S. McCall, and T. Venkatesan, Phys. Rev. Lett. **36**, 1135 (1976).
- [7] F. Shuda, C. Stroud, Jr., and M. Hercher, J. Phys. B **7**, 198 (1974).
- [8] G. Alzetta, A. Gozzini, L. Moi, and G. Orriols, Nuovo Cimento Soc. Ital. Fis., B **36B**, 5 (1976).
- [9] R. Slusher, L. Hollberg, B. Yurke, J. Mertz, and J. Valley, Phys. Rev. Lett. **55**, 2409 (1985).
- [10] P. Liao, J. Bjorkholm, and P. Berman, Phys. Rev. A **20**, 1489 (1979).
- [11] Y. Prior, A. Bogdan, M. Dagenais, and N. Bloembergen, Phys. Rev. Lett. **46**, 111 (1981).
- [12] E. Woodbury and W. Ng, Proc. IRE **50**, 2367 (1962).
- [13] N. Bloembergen, H. Lotem, and R. Lynch, Jr., Indian J. Pure Appl. Phys. **16**, 151 (1978).
- [14] R. Abrams and R. Lind, Opt. Lett. **2**, 94 (1978).
- [15] S. Harris, J. Field, and A. Imamoğlu, Phys. Rev. Lett. **64**, 1107 (1990).
- [16] J.P. Marangos, J. Mod. Opt. **45**, 471 (1998).
- [17] Y. Zhu, Phys. Rev. A **45**, R6149 (1992).
- [18] S. Alam, *Lasers Without Inversion and Electromagnetically Induced Transparency* (SPIE, Bellingham, WA, 1999).
- [19] D. Fulton, S. Shepherd, R. Moseley, B. Sinclair, and M. Dunn, Phys. Rev. A **52**, 2302 (1995).
- [20] R. Miles and S. Harris, IEEE J. Quantum Electron. **9**, 470 (1973).
- [21] V. Wong, R. Boyd, C. Stroud, Jr., R. Bennink, and D. Aronstein, Phys. Rev. A **65**, 013810 (2001).
- [22] D. Steel and J. Remillard, Phys. Rev. A **36**, 4330 (1987).
- [23] H. Schlossberg and A. Javan, Phys. Rev. **150**, 267 (1966).
- [24] S. Mandel and P. Ghosh, Phys. Rev. A **45**, 4990 (1992).
- [25] M. Feld and A. Javan, Phys. Rev. **177**, 540 (1969).
- [26] D. Nikonov, M. Scully, M. Lukin, E. Fry, L. Hollberg, G. Padmabandu, G. Welch, and A. Zibrov, Proc. SPIE **2798**, 342 (1995).
- [27] H. Gray, R. Whitley, and C. Stroud, Jr., Opt. Lett. **3**, 218 (1978).
- [28] J. Eberly, Quantum Semiclassic. Opt. **7**, 373 (1995).
- [29] I. Mazets, B. Matisov, E. Cerboneschi, and E. Arimondo, Phys. Lett. A **229**, 77 (1997).
- [30] H. Xia, S. Sharpe, A. Merriam, and S. Harris, Phys. Rev. A **56**, R3362 (1997).
- [31] F. Renzoni, W. Maichen, L. Windholz, and E. Arimondo, Phys. Rev. A **55**, 3710 (1997).
- [32] D. Budker, D. Orlando, and V. Yashchuk, Am. J. Phys. **67**, 584 (1999).
- [33] K. Motomura and M. Mitsunaga, J. Opt. Soc. Am. B **19**, 2456 (2002).
- [34] A. Lezama, S. Barreiro, A. Lipsich, and A. Akulshin, Phys. Rev. A **61**, 013801 (1999).
- [35] L. Hau, S. Harris, Z. Dutton, and C. Behroozi, Nature **397**, 594 (1999).
- [36] W. Happer, Rev. Mod. Phys. **44**, 169 (1972).
- [37] M. Sargent III, Phys. Rep. **43**, 223 (1978).